JACS
JOURNAL OF THE AMERICAN CHEMICAL SOCIETY
Article
pubs.acs.org/JACS

Are the Crystal Structures of Enantiopure and Racemic Mandelic Acids Determined by Kinetics or Thermodynamics?

Rebecca K. Hylton,[†] Graham J. Tizzard,[‡] Terence L. Threlfall,[‡] Amy L. Ellis,[‡] Simon J. Coles,*[,‡] Colin C. Seaton,[+] Eric Schulze,[§] Heike Lorenz,[§] Andreas Seidel-Morgenstern,[§,∥] Matthias Stein,*[,§] and Sarah L. Price*[,†]

[†]Department of Chemistry, University College London, 20 Gordon Street, London WC1H 0AJ, U.K.
[‡]Chemistry, Faculty of Natural and Environmental Sciences, University of Southampton, Highfield, Southampton SO17 1BJ, U.K.
[+]School of Chemical Engineering and Analytical Science, University of Manchester, The Mill, Oxford Road, Manchester M13 9PL, U.K.
[§]Max-Planck-Institut für Dynamik Komplexer Technischer Systeme, D-39106 Magdeburg, Germany
[∥]Otto-von-Guericke-Universität, Chemische Verfahrenstechnik, D-39106 Magdeburg, Germany

Supporting Information

ABSTRACT: Mandelic acids are prototypic chiral molecules where the sensitivity of crystallized forms (enantiopure/racemic compound/polymorphs) to both conditions and substituents provides a new insight into the factors that may allow chiral separation by crystallization. The determination of a significant number of single crystal structures allows the analysis of 13 enantiopure and 30 racemic crystal structures of 21 (F/Cl/Br/CH_3/CH_3O) substituted mandelic acid derivatives. There are some common phenyl packing motifs between some groups of racemic and enantiopure structures, although they show very different hydrogen-bonding motifs. The computed crystal energy landscape of 3-chloromandelic acid, which has at least two enantiopure and three racemic crystal polymorphs, reveals that there are many more possible structures, some of which are predicted to be thermodynamically more favorable as well as slightly denser than the known forms. Simulations of mandelic acid dimers in isolation, water, and toluene do not differentiate between racemic and enantiopure dimers and also suggest that the phenyl ring interactions play a major role in the crystallization mechanism. The observed crystallization behavior of mandelic acids does not correspond to any simple "crystal engineering rules" as there is a range of thermodynamically feasible structures with no distinction between the enantiopure and racemic forms. Nucleation and crystallization appear to be determined by the kinetics of crystal growth with a statistical bias, but the diversity of the mandelic acid crystallization behavior demonstrates that the factors that influence the kinetics of crystal nucleation and growth are not yet adequately understood.

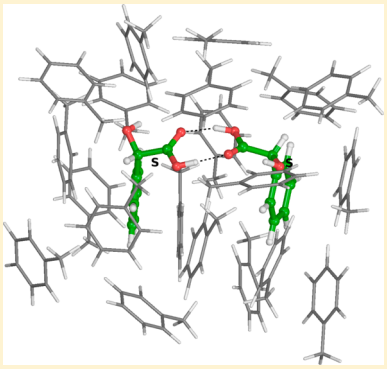

INTRODUCTION

The chirality of biomolecules and their stereospecific recognition by receptors in the human body is linked to fundamental questions about the origins of life and results in our bodies responding differently to molecules that are mirror images of each other. Today, most new small-molecule drugs are chiral; however, the separation of chiral molecules, with many identical physical and chemical properties but a distinct spatial atomic orientation, is a challenge to the chemical and pharmaceutical industries. Chiral resolution by crystallization has many advantages over asymmetric synthesis for the large scale production of enantiopure specialty chemicals.[1] The design of an effective process requires a detailed knowledge of the phase diagram with a solvent suitable to support resolution[2] and exploitation of distinctive characteristics[3] based on an assumption of thermodynamic control of the crystallization process. Racemic mixtures can crystallize in three different ways, by forming either a conglomerate, racemic compound or, less frequently, a pseudoracemate.[4] Which of these is produced strongly influences the way in which the chiral molecules can be separated, with only conglomerates producing a mixture in which the two pure enantiomers can be mechanically separated. However, the assumption that crystallization will result in only one racemic compound or two separate enantiopure crystal structures (i.e., a conglomerate) seems unlikely given the extent of observed[5,6] and potential[7] polymorphism (multiple crystal structures containing the same chemical constituents) for organic molecules. If the experiments lead to the production of long-lived metastable polymorphs of either the racemic or enantiopure crystals, then chiral separation by crystallization runs the risk of the late appearance of a thermodynamically more stable form. This can lead to loss of control of the physical and physiological properties of the process and

Received: June 8, 2015
Published: August 5, 2015

DOI: 10.1021/jacs.5b05938
J. Am. Chem. Soc. 2015, 137, 11095−11104

product. Polymorph screening techniques[8] try to determine all potential crystal structures of a given molecule and have advanced considerably in the past 20 years, but no screening program can guarantee finding all solid forms. Hence computational crystal structure prediction methods are being developed with the aim of helping to identify the most stable forms[9] and to estimate the solubility difference between the racemic and enantiopure crystals. To avoid an extensive research program to determine the potential for chiral separation by crystallization for each molecule, it would be valuable to know whether there are general trends for the existence of alternative crystal structures within families of molecules. How sensitive are racemic and enantiopure crystal structures, their polymorphs, and relative solubilities to small changes in the molecule?

The mandelic acids (Chart 1) are prototypical chiral molecules that are used as antibacterial agents and cosmetics, as well as intermediates in industrial synthesis for many molecules.[10] Hence they require a carefully designed separation process to select the desired enantiomer.[1,11] This family of molecules, with sterically undemanding phenyl ring substituents which do not compete as hydrogen bond donors, were independently chosen as a focus of study by the recent European INTENANT (INTegrated synthesis and purification of single ENANTiomers) project[11,12] and a crystal engineering analysis of the structural systematics of the racemic compounds.[13] In this work, by adding six new enantiopure crystal structures to this series, we are now able to contrast the crystal packing and polymorphism of a large series of enantiopure and racemic crystal structures of mandelic acid derivatives with the same hydrogen-bonding capabilities. We have particularly detailed studies of 3ClMA from the exploration of the binary and ternary phase diagrams[10,14] and characterization by powder X-ray diffraction (PXRD) patterns of two racemic and two enantiopure polymorphs,[14] and our work has identified further polymorphs. Thus, the five distinct structures of 3ClMA, plus the 38 other known crystal structures of substituted mandelic acids, can be contrasted with the computer generated structures for 3ClMA. To what extent does the common hydrogen-bonding capability compete with the different phenyl substituents in controlling the crystal structures? This analysis of the crystal structures of many closely related molecules allows us to discuss various hypotheses that have been put forward as factors that control the preference for crystallization in racemic structures. These affect the design of robust crystallization processes for chiral separation.

Chart 1. (a) Mandelic Acid Family, Where the Phenyl Substituents R2, R3, or R4 Include H, F, Cl, Br, I, CF_3, Me, and OMe[a] and (b) Flexible Torsion Angles in 3ClMA Considered in the Computational Generation of Crystal Structures

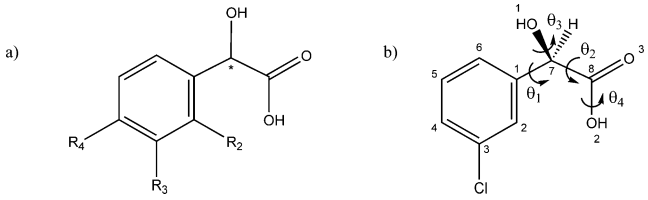

[a]The crystal structures are denoted by chirality (*R*, *S*, or *RS*), the substituents, and the polymorph, for example, S-3ClMA_2.

RESULTS

The diversity of the crystal structures of the set of racemic and enantiopure mandelic acids studied[13] is far greater than in the known structures of 3ClMA shown in Figure 1. All three polymorphs of RS-3ClMA are based on the same hydrogen bonding motif, which includes a hydroxyl−carboxylic acid carbonyl $R_2^2(10)$ dimer (using graph set notation[15] where $R_d^a(r)$ is a ring of r atoms involving a acceptors and d donors). Many other racemic mandelic acids adopt the $R_2^2(8)$ dimer.[13] Form 2 of RS-3ClMA is noteworthy for its isostructural packing (i.e., matching a cluster of the closest 15 molecules) and yet a different crystallographic cell from Form 1.[16] In contrast the newly determined enantiopure crystal structure (S-3ClMA Form 1 in Figure 1) is based on a complex hydrogen-bonded layer including an $R_2^2(9)$ motif with disorder in the Cl positions. This is very different from the Form 2 crystal structure of S-3ClMA, which has four independent molecules in the asymmetric unit cell ($Z' = 4$) and is composed of hydrogen bonding chains that are linked by an $R_3^3(11)$ motif. In the crystallization of the enantiopure mandelic acids, it was generally difficult to obtain diffraction quality crystals.

Comparison of the 13 enantiopure structures shows that they adopt five distinct 3D structures, which are unusually complex (Figure 2), with only S-4FMA having just one molecule in the asymmetric unit cell ($Z' = 1$). The adoption of high Z' structures[17] by the enantiopure crystals could allow the formation of either of the two hydrogen-bonded dimers observed in 27 of the 30 racemic structures[13] (which is not possible for an enantiopure $Z' = 1$ structure), but all the enantiopure crystal structures adopt catemeric hydrogen bonding motifs. XPac[18] analysis of all the mandelic acid crystal structures (Figure 2) seeking any common packing motifs between the enantiopure and racemic crystal structures shows that they have two prevalent one-dimensional packings of the phenyl groups (1D1 and 1D2 in Figure 2). Hence, it appears that the packing of the phenyl groups is critical in determining the crystal structures adopted.

The polymorphism of many of the mandelic acid derivatives demonstrates that the energy differences between the crystal structures may often be small. Several of the racemic polymorphs were found by seeding with crystals of a very similar compound,[13] and metastable conglomerates were obtained by seeding with pure enantiomers of other 2-substituted mandelic acids.[11] However, our extensive experimental search for polymorphs of RS-3ClMA (see SI section 1.3) did not find further polymorphs among the single crystals suitable for synchrotron study, though there is some infrared evidence of further structural diversity.

This extensive series of crystallization experiments on RS-3ClMA was inspired by the computed crystal energy landscape (Figure 3). There are four low energy minima in the conformational energy of isolated 3ClMA (SI Figure 7) defining four distinct types of possible conformational polymorphs.[19] The search in all four conformational regions generated over 3000 plausible $Z' = 1$ crystal structures within 20 kJ mol^{-1} of the most stable calculated crystal structure. As can be observed from the crystal energy landscape (Figure 3), there is no significant difference in the density and relative energies of the racemic and enantiopure crystal structures. This complements the recent observation[20] that the structures in the

DOI: 10.1021/jacs.5b05938
J. Am. Chem. Soc. 2015, 137, 11095−11104

Form and XRD determination	Unit Cell and XPAC construct	Hydrogen Bonding Motif
RS-3-Chloromandelic Acid		
RS Form 1 $P2_1/c$, Z'=1 Single crystal, determined at RT Formed from dissolution in polar aprotic solvents ΔH_f = 17.77 kJ mol^{-1}	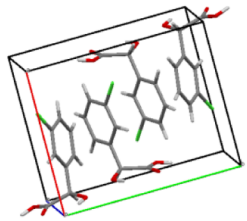 B32	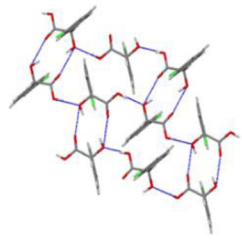 $R_2^2(10)$
RS Form 2 P-1, Z'=2 Single crystal, determined at 100 K Low temperature form, obtained by cooling a single crystal of form 1.	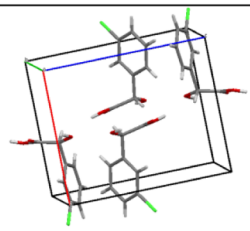 B32	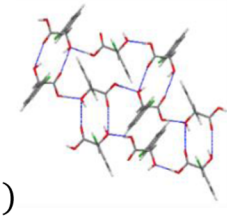 $R_2^2(10)$
RS Form 3 $P2_1/c$, Z'=1 Single crystal, determined at 100 K Obtained by dissolution in dichloromethane ΔH_f = 27.92 kJ mol^{-1}	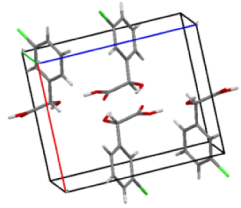 1DB	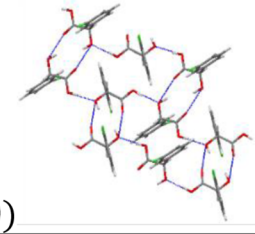 $R_2^2(10)$
S-3-Chloromandelic Acid		
S Form 1 $P2_1$, Z'=2 Single crystal, determined at RT Exhibits phenyl disorder. Obtained by slow solvent evaporation from water ΔH_f = 22.55 kJ mol^{-1}	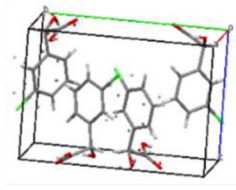 3D4	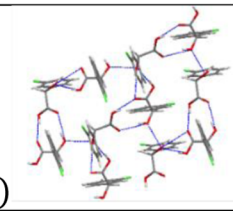 $R_2^2(9)$
S Form 2 $P2_1$, Z'=4 Single crystal, determined at 100 K Crystallized from toluene ΔH_f = 14.62 kJ mol^{-1}	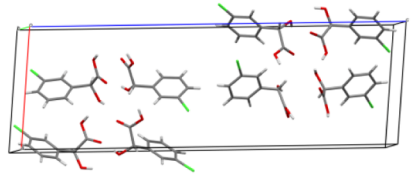 3D2	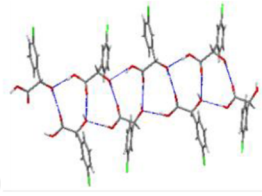 $R_3^3(11)$

Figure 1. An overview of the experimental crystal structures, crystallization conditions (SI, section 1 and refs 14 and 16), and thermodynamic data[14] of 3ClMA.

Cambridge Structural Database show no systematic density differences between the enantiopure and racemic compounds and that the energy differences between racemic and enantiopure compounds are often small, of the same order as polymorphic energy differences, and within the uncertainties of current computational methods.

It is noticeable that the known crystal structures are lower in density and higher in energy than many hypothetical structures. Analyzing the 100 lowest energy structures up to 7 kJ mol^{-1} above the global minimum shows that there are 20 different hydrogen bonding arrangements (SI Table 4), five of which are also observed in the crystal structures of other mandelic acids. All four conformations are observed, with there being many pairs of structures that are identical except for the position of the Cl substituent (i.e., conformation B substituting for A or D for C, SI Figure 7) and close in energy. There are examples of the hydrogen bonding producing an enantiopure ribbon or layer, whose phenyl rings can pack in many ways, producing both racemic and enantiopure structures.

Even though it has been shown to be successful in many other CSP studies,[9] the obvious question is whether this method of evaluating the lattice energy is giving a qualitatively correct picture of the relative stabilities of hypothetical and observed structures. This is answered by comparing the energies of the known metastable crystal structures and six chosen representatives of the hypothetical alternative crystal packings of 3ClMA (Figure 4 and Figure 5), relative to RS-3ClMA_3, evaluated with a range of state-of-the-art computa-

DOI: 10.1021/jacs.5b05938
J. Am. Chem. Soc. 2015, 137, 11095−11104

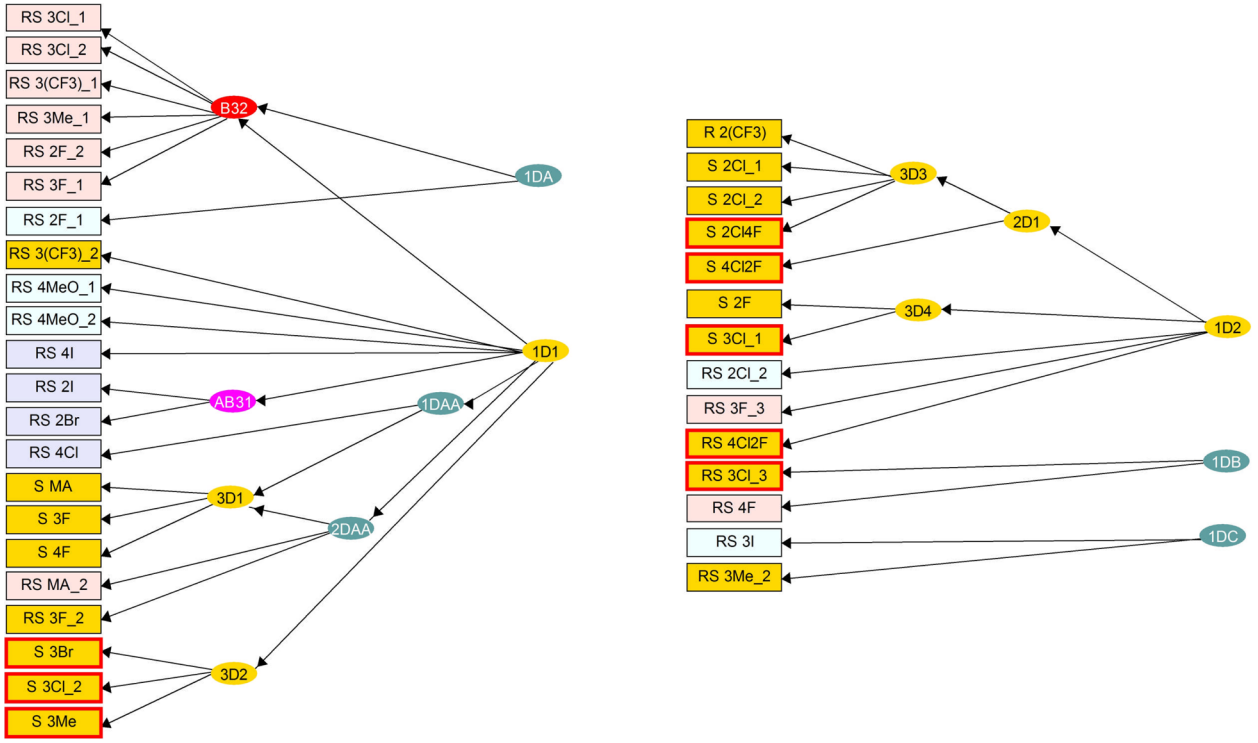

Figure 2. Common packing features of the mandelic acid crystal structures derived from pairwise XPac comparison of enantiopure and racemic crystals. The crystal structures are connected by any common three-dimensional (3D) structures (i.e., isostructural ignoring the substituent), with 3D*x* denoting the isotructural relationships for the enantiopure structures and B32 and AB31 being labels from the previous analysis of just the racemic structures.[13] These are related by any common 2D motifs and finally by the depicted common 1D packing relationships. Packing motif 1D1 is hydrogen−bonded, while 1D2 contains systematic absences. The other 1D relationships are given in SI Figure 2, which also lists the eight crystal structures not on this diagram. The new crystal structures are denoted by a red box. The background color gives the hydrogen bonding motif: yellow for catemer, pink for $R_2^2(8)$, light blue for $R_2^2(10)$, and mauve for both. Only the substituents are given for each of the mandelic acid derivatives, with MA notation omitted for clarity.

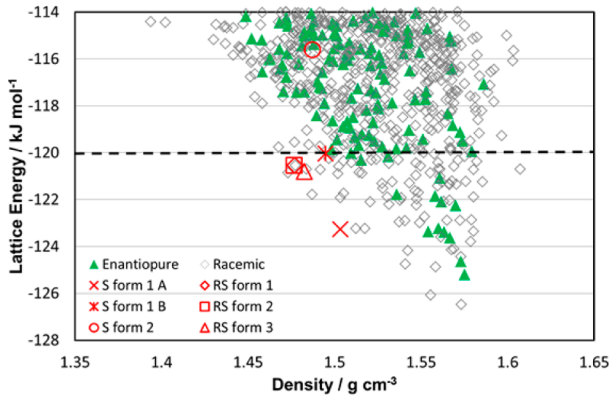

Figure 3. Crystal energy landscape of 3-chloromandelic acid. The enantiopure structures are denoted by green triangles and racemic ones by gray diamonds. The lattice energy minima corresponding to the experimental structures are given in red and were found in the search if $Z' = 1$. Structures shown below the dotted line (at −120 kJ mol^{-1}) were considered in greater detail (SI Table 7).

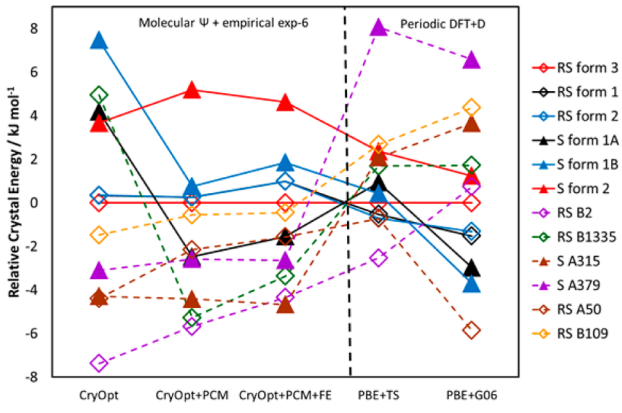

Figure 4. Energies of 3ClMA crystals relative to the most experimentally stable RS Form 3, calculated by different methods: CryOpt, isolated molecule wave functions using *CrystalOptimizer*; + PCM, molecular wave functions calculated in a polarizable continuum (as on Figure 3); + FE, with rigid body free energy estimates; DFT, periodic PBE density functional calculations with + TS (Tkatchenko−Scheffler) and + G06 (Grimme) dispersion corrections. Closed triangles denote enantiopure structures and open diamonds denote racemic structures, with RS forms 1 and 2 frequently superimposed. Observed structures are joined by solid lines and hypothetical ones by dashed lines.

tional methods. The results are generally in agreement with the available experimental data (SI Table 1) with the energy difference between the two disorder components of form 1 of S-3ClMA varying most with computational method. The degree of reranking between different methods, shown in Figure 4, is physically reasonable. The inclusion of environmental effects (either by a polarizable continuum model (PCM) or by periodic electronic structure methods) significantly affects the energy differences between hydrogen bonding motifs. Different dispersion corrections change the relative energies with crystal density. A rigid-body estimate of

DOI: 10.1021/jacs.5b05938
J. Am. Chem. Soc. 2015, 137, 11095−11104

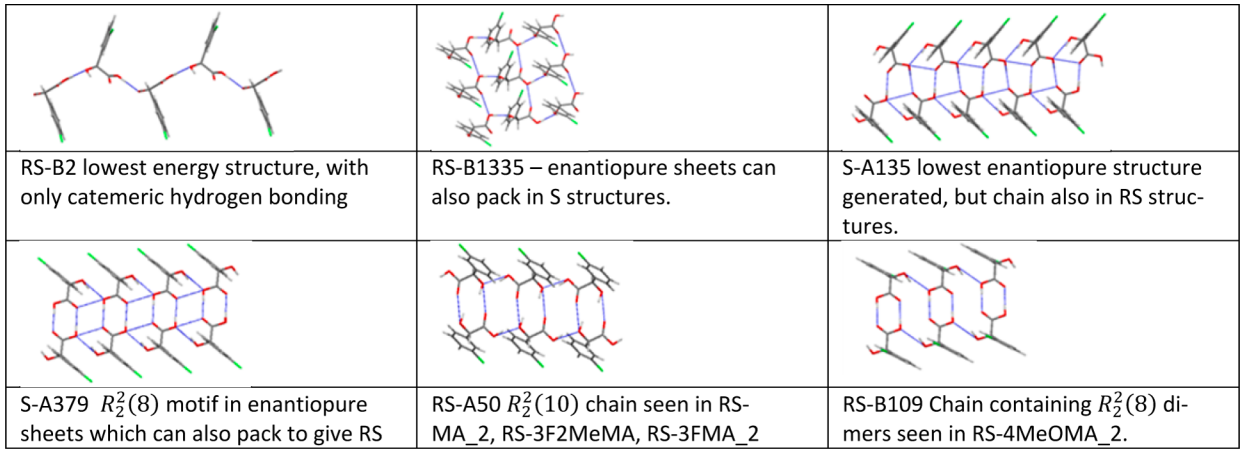

Figure 5. Hydrogen-bonding motif in the hypothetical crystal structures for 3ClMA, whose energies are compared in Figure 4. The letter gives the conformation (A or B, see SI Figure 7) and the number from the energy ranking when the structures were generated by *CrystalPredictor*. The details of these structures are in SI Table 3.

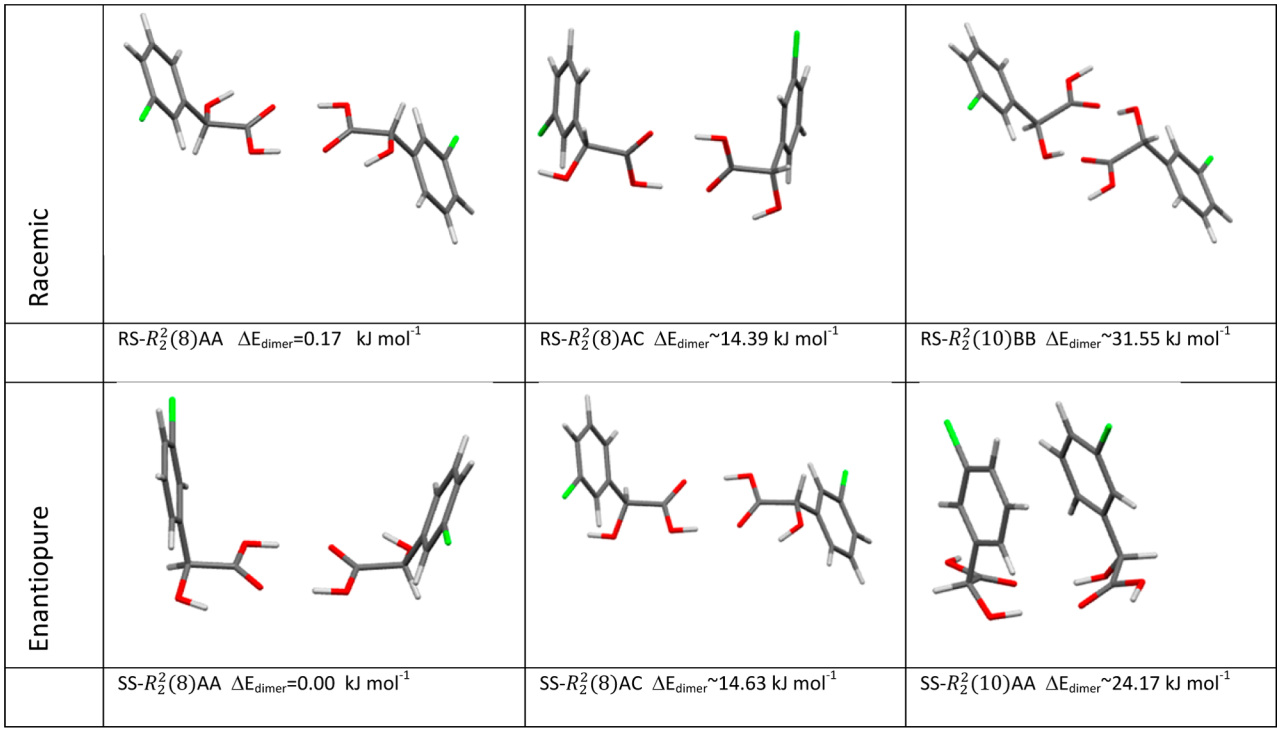

Figure 6. Low energy isolated dimer structures of 3-ClMA, as optimized by counterpoise-corrected MP2 6-31G(d,p) calculations (See SI Table 2 and section 7.1). The binding energies are given relative to the most stable dimer (*SS*-$R_2^2(8)$), which has a binding energy of −56.81 kJ mol^{-1}. The chirality and graph set labels are followed by the two conformer labels, defined by the nearby isolated molecule conformation (SI Figure 7); A is the lowest energy conformation, B has the Cl on the opposite side, which is only 0.07 kJ mol^{-1} higher for the isolated molecule, C and D have the two OH groups on the same side. These labels are also used for mandelic acid dimer types ignoring the Cl.

thermal effects has little effect on relative stability, as is usually the case.[21] The variations in energies are consistent with the challenges in accurately evaluating the lattice energy of even solid benzene to within 1 kJ mol^{-1},[22] and the need for high level treatment of methyl vibrational modes to account for the relative stability of aspirin polymorphs.[23] These uncertainties may account for RS-B2, a structure with a high density and a less conventional hydrogen bonding motif, being the most stable for many computational methods. However, RS-A50 is also close in energy and has the same hydrogen bonding as the three experimentally determined racemic mandelic acid structures based on the $R_2^2(10)$ dimer (see Figure 5). Even hypothetical structures, S-A379 and RS-B109, which contain the hydrogen bonding $R_2^2(8)$ dimer also commonly observed in other racemic mandelic acid structures,[13] are competitive in energy. Hence, there is a detailed and complicated balance between the various inter- and intramolecular forces (conformation, hydrogen bonding, phenyl π stacking, Cl···Cl halogen bonding), which result in diverse, thermodynamically competitive structures for 3ClMA. Thus, it is certain that there are alternative $Z' = 1$ enantiopure as well as racemic structures for 3ClMA that are at least thermodynamically feasible and possibly more stable than the observed structures.

DOI: 10.1021/jacs.5b05938
J. Am. Chem. Soc. 2015, 137, 11095−11104

The differences in hydrogen bonding capabilities and the association of molecules within solution has often been postulated, and sometimes demonstrated, to control the crystal form produced.[24] Quantum chemical calculations on isolated dimers of 3ClMA (Figure 6) show that the $R_2^2(8)$ hydrogen bonding motif is more stable than the $R_2^2(10)$ motif observed in the crystal structures but that the interaction energy is almost independent of whether chirally pure (*SS*) or racemic (*RS*) molecules are their constituents. This has also been found for isolated mandelic acid dimers.[25] However, we note that in most structures the phenyl rings are so distant in the dimers that this is not surprising. Only the *SS*-$R_2^2(10)$ dimer brings the phenyl rings close enough to exhibit a significant dispersion interaction, which is sensitive to the treatment of electron correlation (SI Table 2). Nonetheless, the dimer formation does not account for the observed hydrogen bonding motifs in the RS polymorphs, nor why the enantiopure structures are catemers.

There is still the possibility that the formation of hydrogen-bonded dimers in solution could lead to preformed hydrogen-bonded dimers as effective building blocks in the solid state. However, FTIR studies[25] detect no difference in the racemic or enantiopure solutions and no evidence for association into hydrogen bonding dimers in solutions of methanol, ethanol, DMF, nitromethane, dioxane, and acetonitrile, but some evidence of hydrogen bonding in chloroform. Nitromethane is a nonpolar solvent, like chloroform, and so should not disrupt the formation of hydrogen bonds. However, the solvents were not dried and so the presence of trace amounts of water has the potential to disrupt the hydrogen bonding where it was otherwise expected to be seen.[26] We performed Molecular Dynamics studies of mandelic acid solutions to complement these experiments. Simulations of any of the mandelic acid hydrogen-bonded dimers (*RS* or *SS*, $R_2^2(8)$ or $R_2^2(10)$) in water quickly break up into perfectly solvated separate monomers, producing indistinguishable solutions (SI section 5.1). Simulations in toluene (SI section 5.2), however, show the $R_2^2(8)$ dimer to be the dominant species, but there are fluctuations in the hydrogen bonding reminiscent of the $R_2^2(10)$ dimer observed in the crystal structures. This implies that mandelic acid can easily change hydrogen bonding during crystallization even in the solvents in which it forms dimers. Thus, it appears unlikely that hydrogen bonding in solution persists long enough to play a major role in determining the polymorph. This is consistent with none of the enantiopure structures containing either dimer motif and the majority of the racemic structures containing the $R_2^2(10)$ motif.

The simulations of the mandelic acid dimers in toluene also show no significant difference between the chirally pure (*SS*) and racemic (*RS*) dimers. There are rapid changes from the phenyl rings being on opposite sides (e.g., *RS*-$R_2^2(8)$AA, *RS*-$R_2^2(10)$BB, and *SS*-$R_2^2(8)$AC in Figure 6) to being on the same side of the carboxylic acid group dimer (e.g., *SS*-$R_2^2(8)$AA, *RS*-$R_2^2(8)$AC, *SS*-$R_2^2(10)$AA in Figure 6). The rate of 12.3 ± 3.0 changes per nanosecond for *RS* dimers is the same as for the *SS* dimers of 11.5 ± 3.2 per nanosecond (SI Table 6). There is no significant difference in the rapid rate of phenyl rotation, with 8.6 ± 1.1 rotations per nanosecond for the *RS* and 8.4 ± 1.6 per nanosecond for the *SS* dimer. The rapid phenyl rotation of mandelic acid in water or toluene may explain the chlorine atom positional disorder and the phenyl ring disorder observed in some of the crystal structures. Reorganization of the toluene solvent shell is required to enable phenyl ring rotation. Thus, while the solvent does have an effect on the rate of conformational phenyl ring inversions (SI Table 6) of the monomer and prevalence of hydrogen-bonded dimers, this only helps explain the formation of different polymorphs from different solvents (cf Figure 1 for 3ClMA). The molecular conformations and hydrogen bonding in solution do not appear to direct which crystal structures can be adopted. (We are not considering chiral solvents, which do affect the crystallization of mandelic acid.[27]) In water or toluene, the rotational motions are so fast that it seems unlikely that the crystal growth will be impeded by the rate of interconversion of conformers of isolated molecules or dimers in solution.[28]

DISCUSSION

The simple flexible, chiral 3ClMA has a surprisingly complex crystal energy landscape. Some of the diverse hydrogen bonding motifs and phenyl interactions in the computer generated structures for 3ClMA are seen in the crystal structures for other simply substituted mandelic acids (SI Table 4). The diversity of the observed mandelic acid structures is consistent with both the polymorphism of 3ClMA and the relative computed lattice energies showing no significant thermodynamic advantage for any of observed structures. Indeed the observed structures for 3ClMA may not be the most thermodynamically stable, with simpler and equally plausible hypothetical crystal structures being similar or lower in energy. The solvent affects the hydrogen bonding in solution, and the polymorph formed, but the persistence of hydrogen bonds in solution is not long enough to predetermine the crystal structure formed.

To explain why the observed structures crystallize and particularly why the enantiopure structures crystallize so poorly in such complex structures, when other structures are thermodynamically competitive, we need to consider the kinetics of nucleation and growth. Our results show that the crystallization is not determined by the chiral hydrogen bonding part of the molecule but appears to be strongly influenced by the packing of the phenyl rings. The diversity of mandelic acid structures and lack of similarities in the solid phase behavior[11] is consistent with strong interactions of the differently substituted phenyl groups determining the crystal structure and growth mechanisms. Many of the computer generated thermodynamically favorable structures look statistically unlikely to form from a racemic solution, for example, structures based on enantiopure layers (e.g., RS-B1335, S-A379, Figure 5). The complexity of the observed chiral structures is consistent with them requiring less specific ordering of the substituents (cf the disorder in form 1 of S-3ClMA). The phenyl ring orientation can be swapped in some, but not all, of the 3ClMA computer generated crystal structures with little or no effect on the lattice energy, which explains the differences in crystallization behavior between the symmetric, 4-substituted mandelic acids and the asymmetric ones with 2- and 3-substituents.[11,29] Ordering a 2- or 3-substituted phenyl group during crystal growth will be statistically more difficult. These factors are in addition to a general statistical "collision probability" effect that will favor the formation of racemic over enantiopure nuclei from racemic solutions.[11,20] It is also likely that the opposite enantiomer inhibits the growth of the enantiopure structures, given the effects of related additives.[30] No conglomerate forms from metastable racemic solutions containing phenyl based molecules that selectively inhibit the crystallization of the racemic and not chiral mandelic acid,[31]

DOI: 10.1021/jacs.5b05938
J. Am. Chem. Soc. 2015, 137, 11095−11104

and an additive can promote the crystallization of the metastable conglomerate of 2ClMA.[32] However, the presence of the other enantiomer is not structure determining because we have grown the same enantiopure polymorphs of 3ClMA from racemic solutions, as were found (at least to the discriminating ability of powder X-ray diffraction) in the separation studies.[14]

Previously published unexpected features of the crystallization of mandelic acids[11] support the growth of crystals being a complex balance of the kinetics of desolvation, conformational change, phenyl packing, and hydrogen bonding. The phenyl packing disorder in form 1 of S-3ClMA and its stability relative to the most stable racemic form is a temperature dependent, kinetic effect rather than a thermodynamic effect.[31] The chiral form of mandelic acid does not express any polar surfaces,[33] suggesting a surface chemistry limitation related to the growth being affected by phenyl packing more than hydrogen bonding. Surface structure is very important for the effectiveness of "tailor-made" additives to enhance chiral separation,[34] but inhibition can also occur.

Deliberate seeding with the desired crystal form is usually used in industrial crystallization processes to prevent the production of undesired polymorphs from the stochastic nature of nucleation. In laboratory experiments, all the crystallized sample can arise from a single nucleus, as has been shown to occur in laboratory conditions that should give concomitant polymorphs of 4-hydroxyacetophenone and isonicotinamide.[16] Although considerable efforts are taken in laboratory experiments to avoid seeding with the known form, recent experiments on the nucleation rate of fenoxycarb (which also has aromatic and hydrogen bonding functional groups) show a considerable memory effect unless unusual care is taken with the solution pretreatment.[35] It is rare that a crystallization experiment can be performed starting from an exactly 50:50 solution of enantiomers with solutions that have no memory of the input material.[36] Once crystallization is initiated, Ostwald ripening will occur so that the larger crystals grow at the expense and dissolution of the smaller. Small imbalances in enantiomers thus get magnified in chiral crystallization. The determination of ternary phase diagrams seeks quantitative information about the thermodynamic equilibrium between the solid and liquid phases, which may not favor the appearance of some novel thermodynamically competitive polymorphs.

Heterogeneous seeding can be structure determining for the mandelic acids as shown by our use of isostructural cross-seeding to generate[13] a new polymorph of RS-3MeMA and new metastable conglomerates by seeding with S-2ClMA.[11] Inadvertent seeding particularly through structurally related impurities can also play a major role, as shown particularly dramatically in the case of ritonavir, where heterogeneous nucleation from a degradation product appeared to be responsible for the first appearance of a significantly more stable form.[37] This is just one example of the late appearance and apparent disappearance of polymorphs.[38]

A similar lack of a link between solution chemistry and crystallization outcome has recently been demonstrated for the conformational polymorphs of tolfenamic acid[39] highlighting the challenges in experimentally determining the kinetic factors involved in nucleation and growth. Given the difficulty in obtaining the first diffraction quality crystals of the enantiopure mandelic acids, it seems likely that chance and kinetics play a major role in determining which of the thermodynamically competitive crystal structures crystallizes first. After that, memory effects and inadvertent seeding might favor the growth of the known forms and reduce the chance of observing further polymorphs.

Mandelic acids have long been acknowledged to present more complex crystallization behavior than is usually expected for small organic molecules, despite being the prototype for chiral separation studies. However, their crystal structures being a compromise between molecular flexibility, hydrogen bonding, and van der Waals interactions makes them a prototype for many pharmaceutical molecules, which also have substituted aromatic groups flexibly linked to polar hydrogen bonding regions. Pharmaceuticals often have many thermodynamically equivalent modes of packing. Small changes in substituents or the presence of chemically related impurities can have a dramatic effect on the ability to crystallize a pharmaceutical molecule, let alone its crystal structure. The mandelic acids show the difficulties in understanding nucleation and crystal growth sufficiently well to be able to rationally design a range of experiments to confirm that all practically important polymorphs have been found[5,7,40] or to predict the phase diagrams adequately. However, once this has been achieved, there are potential benefits for the rational design of separation[1] and other crystallization processes[40] to improve the quality of the final product. When the thermodynamic difference between racemic and enantiopure forms and their polymorphs is small, there is a potential advantage that the kinetic factors may be more readily controlled by appropriate choice of solvent, temperature, and seeding to drive a satisfactory process.

■ CONCLUSIONS

This overview of the enantiopure and racemic crystal structures adopted by simply substituted mandelic acids reveals that a wide range of crystal packings are observed and thermodynamically competitive. The packing of the phenyl groups (which is affected by the substituents) balances with a variety of hydrogen bonding motifs and conformational flexibility to give structural diversity. This diversity defies simple explanations of chiral crystallization. Our experimental work has found a significant degree of polymorphism, though even in the case of racemic 3ClMA, the screening is far from complete by industrial standards. Nonetheless, the relationship between the computed crystal energy landscape for 3ClMA and the diversity of substituted mandelic acid crystal structures raises the question of why simpler enantiopure and more forms of racemic mandelic acids have not been found so far.

Analyzing the new enantiopure crystal structures in contrast with the racemic structures shows that phenyl packing is strongly affecting crystal nucleation and growth. Statistical probability also plays a role in determining which structures are found and in the difficulty in crystallizing the enantiopure structures. The association of molecules in some solvents is not sufficiently strong to determine the crystal structures. There is a substitution-dependent struggle to pack the phenyl groups correctly during crystal growth, while simultaneously forming various hydrogen bonding motifs. The formation of the initial nucleus is therefore a key step in determining which structures are formed. Some computer-generated thermodynamically plausible crystal structures are statistically unlikely to form, though this might occur in the presence of specific impurities or surfaces. Understanding nucleation well enough to determine whether a given thermodynamically favorable crystal structure can be made to nucleate is a fundamental scientific challenge. In practice, seeding and Ostwald ripening play a significant role in

DOI: 10.1021/jacs.5b05938
J. Am. Chem. Soc. 2015, 137, 11095−11104

ensuring that crystallization usually results in only one racemic and one enantiopure phase.

A compensating advantage of crystallization being a subtle and complex balance of competing kinetic effects of nucleation and growth between thermodynamically competitive structures is the potential for finding new solid forms with improved physical properties. It also allows the design of processes for chiral separation[1] of a wider range of molecules by careful tailoring of conditions.

MATERIALS AND METHODS

The materials and methods used to produce all of the crystal structures reported, except RS-3ClMA form 3, have been previously reported by the Magdeburg group.[11,41]

RS-3ClMA form 3 has a $P2_1/c$, $Z' = 1$, structure with a = 8.6234(12) Å, b = 10.4812(14) Å, c = 9.3924(13) Å, β = 93.846(7)°, and V = 847.007 Å^3. The single crystal was obtained from dichloromethane, from material produced via cyanohydrin synthesis from 3-Cl benzaldehyde sourced from Alfa. The crystals of S-3ClMA form 1 ($P2_1$, $Z' = 2$, crystals; a = 8.3160(18) Å, b = 11.855(3) Å, c = 8.4526(18) Å, β = 93.820(7)°, and V = 831.458 Å^3) exhibit full molecule disorder in the ratio 2:1. The major and minor component are both ordered crystal structures containing the molecule with bond lengths and angles close to those observed in other 3ClMA structures, so two ordered models can be derived for calculations, differing in the placement and geometry of the second molecule, denoted S-3ClMA form 1_A and S-3ClMA form 1_B for the major and minor components, respectively. S-3ClMA form 2 is a $P2_1$, $Z' = 4$, structure with a = 9.8701(8) Å, b = 5.4344(6) Å, c = 30.656(2) Å, β = 95.260(8)°, and V = 1637.4 Å^3.

The other new mandelic acid crystal structures are S-3MeMA, a $P2_1$, $Z' = 4$, structure with a = 10.0845(9) Å, b = 5.3717(5) Å, c = 30.358(4) Å, β = 91.800(12)°, and V = 1643.71 Å^3; S-3BrMA, a $P2_1$, $Z' = 4$, structure with a = 9.7454(19) Å, b = 5.5417(6) Å, c = 31.396(4) Å, β = 95.094(15)°, and V = 1688.88 Å^3; S-2Cl4FMA, a $P2_1$, $Z' = 2$, structure with a = 7.8577(8) Å, b = 7.8314(6) Å, c = 14.1039(12) Å, β = 105.477(10)°, and V = 836.436 Å^3; S-4Cl2FMA having whole molecule disorder in a $P2_1$, $Z' = 2$, structure with a = 7.9508(7) Å, b = 7.0951(9) Å, c = 15.8626(15) Å, β = 95.565(9)°, and V = 890.619 Å^3; and RS-4Cl2FMA, a $P\bar{1}$, $Z' = 4$, structure with a = 7.7848(5) Å, b = 13.5323(10) Å, c = 16.7476(18) Å, α = 96.955(8)°, β = 99.289(8)°, γ = 90.680(6)°, and V = 1727.46 Å^3.

Computational Methods. Crystal structures were compared in a pairwise fashion using XPac,[18] using the non-hydrogenic atoms of mandelic acid to determine whether there were any supramolecular constructs in common between the enantiopure and racemic structures. This supplements the analysis of the racemic structures.[13] The 3ClMA structures were also visualized and overlaid using the Crystal Packing Similarity tools in Mercury.[42]

The flexibility of 3ClMA leads to four local conformational minima (SI Figure 7) and a wide range of the flexible torsion angles (Chart 1) that are sufficiently low in energy to be possible crystal conformations.[19] The search was based on separating the lattice energy into the intermolecular contribution, U_{inter}, and the energy penalty, ΔE_{intra}, for changing the molecular conformation, that is, $E_{latt} = U_{inter} + \Delta E_{intra}$.[43] Ab initio calculations on the isolated molecule using Gaussian03[44] at the MP2/6-31G(d,p) level were used for ΔE_{intra} and were analyzed by GDMA to give the distributed multipole representation of the charge density[45] used in DMACRYS[43] for the electrostatic component of the lattice energy. All other intermolecular energies were represented by an isotropic atom−atom exp-6 potential, using the parameters of the FIT potential.[43]

CrystalPredictor[46] was used to generate approximately one million $Z' = 1$ crystal structures in each conformational region. The most promising 3500 unique structures were refined using *CrystalOptimizer*.[47] Full details and the crystal energy landscape at this stage are in SI Figure 8. To approximate the effect of the crystalline environment on the charge distribution and conformational energies,[48] we estimated the effect of polarization through a polarizable continuum model (PCM)[49] using the MP2 wave function with a dielectric constant of $\varepsilon = 3$. This is the crystal energy landscape in Figure 3. To estimate the effects of temperature on the relative stability, a rigid molecule harmonic estimate of the Helmholtz free energy, including the zero-point vibrational energy,[50] was made from the elastic constants[51] and $k = 0$[52] phonons.

Alternative estimates of the lattice energy were obtained using periodic electronic structure calculations, namely, a plane wave DFT-D approach using the CASTEP[53] code with the PBE functional and either a Grimme (G06)[54] or Tkatchenko−Scheffler (TS)[55] dispersion correction with full optimization.

Estimates of the binding energy of the dimers in isolation were performed using Gaussian03 using MP2 perturbation theory and a 6-31G(d,p) basis set and corrected for the basis set superposition error with the Counterpoise keyword.

The solution simulations started from quantum chemically optimized dimer structures of *R*- and *S*-mandelic acid positioned in the center of a cubic box of dimensions 30 × 30 × 30 Å^3 for water and 45 × 45 × 45 Å^3 for toluene. Parametrization of the mandelic acid molecules was done with ParamChem0.9.7.1beta.[56] The mandelic acid dimers were solvated in explicit TIP3 water[57] using VMD. 1.9.1[58] and its solvate plugin 2 and in explicit toluene using an internal protocol; 782 water molecules and 498 toluene molecules were positioned in a radius of 3 Å around the solutes. Molecular dynamics simulations were performed using NAMD 2.9[59] with the CHARMM36 force field[60] and the CGenFF2B8 force field for small molecules.[61] A nonbonding a cutoff of 12 Å, a switch distance of 10 Å, and a pair list distance of 14 Å were set. Every simulation was done in a NVT-ensemble at 293 K, controlled by a Langevin Thermostat[62] with a damping coefficient of 1/ps and coupled hydrogens. Periodic boundary conditions were applied. Interactions were computed using the PME method[63] with a grid of 60 × 60 × 60 Å^3 for water and 90 × 90 × 90 Å^3 for toluene. The integrator utilized a time step of 1 fs, the nonbonded interactions were computed at every step, and the atoms were reassigned every 20 steps. The system setup was minimized for 5000 steps, and production runs ran for 10^7 steps (10 ns). The trajectory was collected every 2500 steps.

ASSOCIATED CONTENT

Supporting Information

The Supporting Information is available free of charge on the ACS Publications website at DOI: 10.1021/jacs.5b05938.

Crystal structures (CIF)

Experimental and computational details as reported in the text (PDF)

AUTHOR INFORMATION

Corresponding Authors

*s.l.price@ucl.ac.uk

*matthias.stein@mpi-magdeburg.mpg.de

*s.j.coles@soton.ac.uk

Present Address

Current address for Colin Seaton: School of Chemistry and Forensic Science, University of Bradford, Bradford BD7 1DB, U.K.

Notes

The authors declare no competing financial interest.

ACKNOWLEDGMENTS

We thank Dr. Tam Le Minh and Dr. Jan von Langermann for preparation and provision of samples of different mandelic acid derivatives. Periodic DFT calculations were performed on ARCHER, the UK's national high-performance computing service, via our membership of the UK's HPC Materials

DOI: 10.1021/jacs.5b05938
J. Am. Chem. Soc. 2015, 137, 11095−11104

Chemistry Consortium, which is funded by EPSRC (**EP/L000202**). ARCHER is funded by the Office of Science and Technology through EPSRC's High End Computing Programme. Financial support from the Max Planck Society for the Advancement of Sciences is gratefully acknowledged. R.K.H. is grateful for a UCL-MPS Impact Ph.D. Fellowship. This work was also supported in part by ESPRC EP/K039229/1 and the EU COST Action CM1402 "Crystallize".

REFERENCES

(1) Lorenz, H.; Seidel-Morgenstern, A. *Angew. Chem., Int. Ed.* **2014**, *53*, 1218−1250.
(2) Lorenz, H.; Seidel-Morgenstern, A. *Thermochim. Acta* **2002**, *382*, 129−142.
(3) Lorenz, H.; Perlberg, A.; Sapoundjiev, D.; Elsner, M. P.; Seidel-Morgenstern, A. *Chem. Eng. Process.* **2006**, *45*, 863−873. Le Minh, T.; Lorenz, H.; Seidel-Morgenstern, A. *Chem. Eng. Technol.* **2012**, *35*, 1003−1008. Jacques, J.; Collet, A.; Wilen, S. H. *Enantiomers, Racemates and Resolutions*; Wiley-Interscience: New York, 1981. Beilles, S.; Cardinael, P.; Ndzie, E.; Petit, S.; Coquerel, G. *Chem. Eng. Sci.* **2001**, *56*, 2281−2294.
(4) Roozeboom, H. W. B. *Z. Phys. Chem.* **1899**, *28*, 494−517.
(5) Bernstein, J. *Cryst. Growth Des.* **2011**, *11*, 632−650.
(6) Lee, A. Y.; Erdemir, D.; Myerson, A. S. *Annu. Rev. Chem. Biomol. Eng.* **2011**, *2*, 259−280. Desiraju, G. R. *Cryst. Growth Des.* **2008**, *8*, 3−5.
(7) Price, S. L. *Acta Crystallogr., Sect. B: Struct. Sci., Cryst. Eng. Mater.* **2013**, *69*, 313−328.
(8) Newman, A. *Org. Process Res. Dev.* **2013**, *17*, 457−471.
(9) Price, S. L. *Chem. Soc. Rev.* **2014**, *43*, 2098−2111. Braun, D. E.; McMahon, J. A.; Koztecki, L. H.; Price, S. L.; Reutzel-Edens, S. M. *Cryst. Growth Des.* **2014**, *14*, 2056−2072. Ismail, S. Z.; Anderton, C. L.; Copley, R. C.; Price, L. S.; Price, S. L. *Cryst. Growth Des.* **2013**, *13*, 2396−2406.
(10) Zhang, Y.; Ray, A.; Rohani, S. *Chem. Eng. Sci.* **2009**, *64*, 192−197.
(11) von Langermann, J.; Temmel, E.; Seidel-Morgenstern, A.; Lorenz, H. *J. Chem. Eng. Data* **2015**, *60*, 721−728.
(12) Seidel-Morgenstern, A. INTENANT Report Summary. http://cordis.europa.eu/result/report/rcn/45395_en.html 2010. Federsel, H. J. *Org. Process Res. Dev.* **2012**, *16*, 260−261.
(13) Coles, S.; Ellis, A.; Leung, K.; Sarson, J.; Threlfall, T.; Tizzard, G. *CrystEngComm* **2014**, *16*, 10816−10823.
(14) Le Minh, T.; von Langermann, J.; Lorenz, H.; Seidel-Morgenstern, A. *J. Pharm. Sci.* **2010**, *99*, 4084−4095.
(15) Bernstein, J.; Davis, R. E.; Shimoni, L.; Chang, N. *Angew. Chem., Int. Ed. Engl.* **1995**, *34*, 1555−1573.
(16) Coles, S. J.; Threlfall, T. L.; Tizzard, G. J. *Cryst. Growth Des.* **2014**, *14*, 1623−1628.
(17) Steed, K. M.; Steed, J. W. *Chem. Rev.* **2015**, *115*, 2895−2933. Anderson, K. M.; Goeta, A. E.; Steed, J. W. *Cryst. Growth Des.* **2008**, *8*, 2517−2524. Desiraju, G. R. *CrystEngComm* **2007**, *9*, 91−92.
(18) Gelbrich, T.; Hursthouse, M. B. *CrystEngComm* **2005**, *7*, 324−336.
(19) Cruz-Cabeza, A. J.; Bernstein, J. *Chem. Rev.* **2014**, *114*, 2170−2191.
(20) Gavezzotti, A.; Rizzato, S. *J. Org. Chem.* **2014**, *79*, 4809−4816.
(21) Nyman, J.; Day, G. M. *CrystEngComm* **2015**, *17*, 5154−5165.
(22) Yang, J.; Hu, W.; Usvyat, D.; Matthews, D.; Schutz, M.; Chan, H. *Science* **2014**, *345*, 640−643.
(23) Reilly, A.; Tkatchenko, A. *Phys. Rev. Lett.* **2014**, *113*, 055701.
(24) Kulkarni, S. A.; McGarrity, E. S.; Meekes, H.; ter Horst, J. H. *Chem. Commun.* **2012**, *48*, 4983−4985. Khamar, D.; Zeglinski, J.; Mealey, D.; Rasmuson, Å. C. *J. Am. Chem. Soc.* **2014**, *136*, 11664−11673.
(25) Davey, R. J.; Dent, G.; Mughal, R. K.; Parveen, S. *Cryst. Growth Des.* **2006**, *6*, 1788−1796.
(26) Hamad, S.; Moon, C.; Catlow, C. R. A.; Hulme, A. T.; Price, S. L. *J. Phys. Chem. B* **2006**, *110*, 3323−3329.
(27) Tulashie, S. K.; von Langermann, J.; Lorenz, H.; Seidel-Morgenstern, A. *Cryst. Growth Des.* **2011**, *11*, 240−246.
(28) Derdour, L.; Skliar, D. *Chem. Eng. Sci.* **2014**, *106*, 275−292.
(29) Hursthouse, M. B.; Huth, L. S.; Threlfall, T. L. *Org. Process Res. Dev.* **2009**, *13*, 1231−1240.
(30) Robin, A.; Iavicoli, P.; Wurst, K.; Dyer, M.; Haq, S.; Amabilino, D.; Raval, R. *Cryst. Growth Des.* **2010**, *10*, 4516−4525.
(31) Mughal, R. K.; Davey, R. J.; Blagden, N. *Cryst. Growth Des.* **2007**, *7*, 218−224.
(32) Davey, R. J.; Sadiq, G.; Back, K.; Wilkinson, L.; Seaton, C. C. *Chem. Commun.* **2012**, *48*, 1976−1978.
(33) Mughal, R. K.; Davey, R. J.; Black, S. N. *Cryst. Growth Des.* **2007**, *7*, 225−228.
(34) Weissbuch, I.; Addadi, L.; Leiserowitz, L. *Science* **1991**, *253*, 637−645. Weissbuch, I.; Lahav, M.; Leiserowitz, L. *Cryst. Growth Des.* **2003**, *3*, 125−150. Schmidt, C.; Jones, M. J.; Ulrich, J. In *Crystallization: Basic Concepts and Industrial Applications*; Beckmann, W., Ed.; Wiley-VCH Verlag GmbH & Co. KGaA: Weinheim, Germany, 2013; pp 105−127.
(35) Kuhs, M.; Zeglinski, J.; Rasmuson, A. C. *Cryst. Growth Des.* **2014**, *14*, 905−915.
(36) Kulkarni, S.; Meekes, H.; ter Horst, J. *Cryst. Growth Des.* **2014**, *14*, 1493−1499.
(37) Bauer, J.; Spanton, S.; Henry, R.; Quick, J.; Dziki, W.; Porter, W.; Morris, J. *Pharm. Res.* **2001**, *18*, 859−866.
(38) Bučar, D.-K.; Lancaster, R. W.; Bernstein, J. *Angew. Chem., Int. Ed.* **2015**, *54*, 6972−6993.
(39) Du, W.; Cruz-Cabeza, A.; Woutersen, S.; Davey, R.; Yin, Q. *Chemical Science* **2015**, *6*, 3515−3524.
(40) Chen, J.; Sarma, B.; Evans, J. M. B.; Myerson, A. S. *Cryst. Growth Des.* **2011**, *11*, 887−895.
(41) von Langermann, J.; Le Minh, T.; Lorenz, H.; Seidel-Morgenstern, A. *Chem. Ing. Tech.* **2010**, *82*, 93−100.
(42) Macrae, C. F.; Bruno, I. J.; Chisholm, J. A.; Edgington, P. R.; McCabe, P.; Pidcock, E.; Rodriguez-Monge, L.; Taylor, R.; van de Streek, J.; Wood, P. A. *J. Appl. Crystallogr.* **2008**, *41*, 466−470.
(43) Price, S. L.; Leslie, M.; Welch, G. W. A.; Habgood, M.; Price, L. S.; Karamertzanis, P. G.; Day, G. M. *Phys. Chem. Chem. Phys.* **2010**, *12*, 8478−8490.
(44) Frisch, M. J.; Trucks, G. W.; Schlegel, H. B.; Scuseria, G. E.; Robb, M. A.; Cheeseman, J. R.; Montgomery, J. A., Jr.; Vreven, T.; Kudin, K. N.; Burant, J. C.; Millam, J. M.; Iyengar, S. S.; Tomasi, J.; Barone, V.; Mennucci, B.; Cossi, M.; Scalmani, G.; Rega, N.; Petersson, G. A.; Nakatsuji, H.; Hada, M.; Ehara, M.; Toyota, K.; Fukuda, R.; Hasegawa, J.; Ishida, M.; Nakajima, T.; Honda, Y.; Kitao, O.; Nakai, H.; Klene, M.; Li, X.; Knox, J. E.; Hratchian, H. P.; Cross, J. B.; Bakken, V.; Adamo, C.; Jaramillo, J.; Gomperts, R.; Stratmann, R. E.; Yazyev, O.; Austin, A. J.; Cammi, R.; Pomelli, C.; Ochterski, J. W.; Ayala, P. Y.; Morokuma, K.; Voth, G. A.; Salvador, P.; Dannenberg, J. J.; Zakrzewski, V. G.; Dapprich, S.; Daniels, A. D.; Strain, M. C.; Farkas, O.; Malick, D. K.; Rabuck, A. D.; Raghavachari, K.; Foresman, J. B.; Ortiz, J. V.; Cui, Q.; Baboul, A. G.; Clifford, S.; Cioslowski, J.; Stefanov, B. B.; Liu, G.; Liashenko, A.; Piskorz, P.; Komaromi, I.; Martin, R. L.; Fox, D. J.; Keith, T.; Al-Laham, M. A.; Peng, C. Y.; Nanayakkara, A.; Challacombe, M.; Gill, P. M. W.; Johnson, B.; Chen, W.; Wong, M. W.; Gonzalez, C.; Pople, J. A. *Gaussian 03*; Gaussian, Inc.: Wallingford, CT, 2003.
(45) Stone, A. J. *J. Chem. Theory Comput.* **2005**, *1*, 1128−1132. Stone, A. J. *GDMA: A Program for Performing Distributed Multipole Analysis of Wave Functions Calculated Using the Gaussian Program System*, version 2.2; University of Cambridge: Cambridge, United Kingdom, 2010.
(46) Karamertzanis, P. G.; Pantelides, C. C. *Mol. Phys.* **2007**, *105*, 273−291. Vasileiadis, M.; Kazantsev, A. V.; Karamertzanis, P. G.; Adjiman, C. S.; Pantelides, C. C. *Acta Crystallogr., Sect. B: Struct. Sci.* **2012**, *68*, 677−685.

DOI: 10.1021/jacs.5b05938
J. Am. Chem. Soc. 2015, 137, 11095−11104

(47) Kazantsev, A. V.; Karamertzanis, P. G.; Adjiman, C. S.; Pantelides, C. C. *J. Chem. Theory Comput.* **2011**, *7*, 1998−2016.
(48) Habgood, M.; Price, S. L.; Portalone, G.; Irrera, S. *J. Chem. Theory Comput.* **2011**, *7*, 2685−2688. Karamertzanis, P. G.; Day, G. M.; Welch, G. W. A.; Kendrick, J.; Leusen, F. J. J.; Neumann, M. A.; Price, S. L. *J. Chem. Phys.* **2008**, *128*, 244708−244717.
(49) Cooper, T. G.; Hejczyk, K. E.; Jones, W.; Day, G. M. *J. Chem. Theory Comput.* **2008**, *4*, 1795−1805.
(50) Anghel, A. T.; Day, G. M.; Price, S. L. *CrystEngComm* **2002**, *4*, 348−355.
(51) Day, G. M.; Price, S. L.; Leslie, M. *Cryst. Growth Des.* **2001**, *1*, 13−27.
(52) Day, G. M.; Price, S. L.; Leslie, M. *J. Phys. Chem. B* **2003**, *107*, 10919−10933.
(53) Clark, S. J.; Segall, M. D.; Pickard, C. J.; Hasnip, P. J.; Probert, M. J.; Refson, K.; Payne, M. C. *Z. Kristallogr.* **2005**, *220*, 567−570.
(54) Grimme, S. *J. Comput. Chem.* **2006**, *27*, 1787−1799.
(55) Tkatchenko, A.; Scheffler, M. *Phys. Rev. Lett.* **2009**, *102*, 073005.
(56) Vanommeslaeghe, K.; MacKerell, A. *J. Chem. Inf. Model.* **2012**, *52*, 3144−3154. Vanommeslaeghe, K.; Raman, E. P.; MacKerell, A. *J. Chem. Inf. Model.* **2012**, *52*, 3155−3168.
(57) Jorgensen, W. L.; Chandrasekhar, J.; Madura, J. D.; et al. *J. Chem. Phys.* **1983**, *79*, 926−935.
(58) Humphrey, W.; Dalke, A.; Schulten, K. *J. Mol. Graphics* **1996**, *14*, 33−38.
(59) Nelson, M. T.; Humphrey, W.; Gursoy, A.; Dalke, A.; Kale, L. V.; Skeel, R. D.; Schulten, K. *Int. J. Supercomputer Applic. High Perform. Comput.* **1996**, *10*, 251−268. Phillips, J. C.; Braun, R.; Wang, W.; Gumbart, J.; Tajkhorshid, E.; Villa, E.; Chipot, C.; Skeel, R. D.; Kale, L.; Schulten, K. *J. Comput. Chem.* **2005**, *26*, 1781−1802.
(60) Brooks, B. R.; Bruccoleri, R. E.; Olafson, B. D.; States, D. J.; Swaminathan, S.; Karplus, M. *J. Comput. Chem.* **1983**, *4*, 187−217. Best, R. B.; Zhu, X.; Shim, J.; Lopes, P. E.; Mittal, J.; Feig, M.; MacKerell, A. D. *J. Chem. Theory Comput.* **2012**, *8*, 3257−3273.
(61) Vanommeslaeghe, K.; Hatcher, E.; Acharya, C.; Kundu, S.; Zhong, S.; Shim, J.; Darian, E.; Guvench, O.; Lopes, P.; Vorobyov, I.; Mackerell, A. D. *J. Comput. Chem.* **2010**, *31*, 671−690. Yu, W.; He, X.; Vanommeslaeghe, K.; MacKerell, A. D. *J. Comput. Chem.* **2012**, *33*, 2451−2468.
(62) Izaguirre, J. A.; Catarello, D. P.; Wozniak, J. M.; Skeel, R. D. *J. Chem. Phys.* **2001**, *114*, 2090−2098.
(63) Cheatham, T. E.; Miller, J. L.; Fox, T.; Darden, T. A.; Kollman, P. A. *J. Am. Chem. Soc.* **1995**, *117*, 4193−4194.

DOI: 10.1021/jacs.5b05938
J. Am. Chem. Soc. 2015, 137, 11095−11104